



Regional cortical thinning, demyelination and iron loss in cerebral small vessel disease

Hao Li,¹ Mina A. Jacob,¹ Mengfei Cai,^{1,2} Marco Duering,^{3,4} Maxime Chamberland,⁵ David G. Norris,⁵ Roy P. C. Kessels,^{6,7,8} Frank-Erik de Leeuw,¹ José P. Marques⁵ and Anil M. Tuladhar¹

The link between white matter hyperintensities (WMH) and cortical thinning is thought to be an important pathway by which WMH contributes to cognitive deficits in cerebral small vessel disease (SVD). However, the mechanism behind this association and the underlying tissue composition abnormalities are unclear. The objective of this study is to determine the association between WMH and cortical thickness, and the *in vivo* tissue composition abnormalities in the WMH-connected cortical regions.

In this cross-sectional study, we included 213 participants with SVD who underwent standardized protocol including multimodal neuroimaging scans and cognitive assessment (i.e. processing speed, executive function and memory). We identified the cortex connected to WMH using probabilistic tractography starting from the WMH and defined the WMH-connected regions at three connectivity levels (low, medium and high connectivity level). We calculated the cortical thickness, myelin and iron of the cortex based on T₁-weighted, quantitative R1, R2* and susceptibility maps. We used diffusion-weighted imaging to estimate the mean diffusivity of the connecting white matter tracts. We found that cortical thickness, R1, R2* and susceptibility values in the WMH-connected regions were significantly lower than in the WMH-unconnected regions (all $P_{corrected} < 0.001$). Linear regression analyses showed that higher mean diffusivity of the connecting white matter tracts were related to lower thickness ($\beta = -0.30$, $P_{corrected} < 0.001$), lower R1 ($\beta = -0.26$, $P_{corrected} = 0.001$), lower R2* ($\beta = -0.32$, $P_{corrected} < 0.001$) and lower susceptibility values ($\beta = -0.39$, $P_{corrected} < 0.001$) of WMH-connected cortical regions at high connectivity level. In addition, lower scores on processing speed were significantly related to lower cortical thickness ($\beta = 0.20$, $P_{corrected} = 0.030$), lower R1 values ($\beta = 0.20$, $P_{corrected} = 0.006$), lower R2* values ($\beta = 0.29$, $P_{corrected} = 0.006$) and lower susceptibility values ($\beta = 0.19$, $P_{corrected} = 0.024$) of the WMH-connected regions at high connectivity level, independent of WMH volumes and the cortical measures of WMH-unconnected regions.

Together, our study demonstrated that the microstructural integrity of white matter tracts passing through WMH is related to the regional cortical abnormalities as measured by thickness, R1, R2* and susceptibility values in the connected cortical regions. These findings are indicative of cortical thinning, demyelination and iron loss in the cortex, which is most likely through the disruption of the connecting white matter tracts and may contribute to processing speed impairment in SVD, a key clinical feature of SVD. These findings may have implications for finding intervention targets for the treatment of cognitive impairment in SVD by preventing secondary degeneration.

- 1 Department of Neurology, Donders Center for Medical Neurosciences, Radboud University Medical Center, 6500 HB Nijmegen, The Netherlands
- 2 Department of Neurology, Guangdong Neuroscience Institute, Guangdong Provincial People's Hospital, Guangdong Academy of Medical Sciences, Southern Medical University, 510080 Guangzhou, China
- 3 Medical Image Analysis Center (MIAC AG) and Department of Biomedical Engineering, University of Basel, 4051 Basel, Switzerland
- 4 LMU Munich, University Hospital, Institute for Stroke and Dementia Research (ISD), 81377 Munich, Germany

Received March 20, 2023. Revised June 07, 2023. Accepted June 11, 2023. Advance access publication June 27, 2023

© The Author(s) 2023. Published by Oxford University Press on behalf of the Guarantors of Brain.

This is an Open Access article distributed under the terms of the Creative Commons Attribution-NonCommercial License (<https://creativecommons.org/licenses/by-nc/4.0/>), which permits non-commercial re-use, distribution, and reproduction in any medium, provided the original work is properly cited. For commercial re-use, please contact journals.permissions@oup.com

- 5 Donders Institute for Brain, Cognition and Behaviour, Center for Cognitive Neuroimaging, Radboud University, 6525 EN Nijmegen, The Netherlands
- 6 Department of Medical Psychology and Radboudumc Alzheimer Center, Radboud University Medical Center, 6525 GC, Nijmegen, The Netherlands
- 7 Donders Institute for Brain, Cognition and Behaviour, Radboud University, 6525 EN Nijmegen, The Netherlands
- 8 Vincent van Gogh Institute for Psychiatry, 5803 AC Venray, The Netherlands

Correspondence to: Anil M. Tuladhar, MD, PhD
 Department of Neurology (910)
 Radboud University Medical Center
 Reinier Postlaan 4, PO Box 9101, 6500 HB Nijmegen, The Netherlands
 E-mail: Anil.Tuladhar@radboudumc.nl

Keywords: white matter hyperintensities; cortical thickness; myelination; iron; secondary degeneration

Introduction

Cerebral small vessel disease (SVD) is a disease that affects small vessels of the brain and is the leading cause of vascular cognitive impairment and dementia.^{1,2} The features of SVD seen on MRI include white matter hyperintensities (WMH), lacunes of presumed vascular origin, and cerebral microbleeds (CMBs), with WMH being the most common and prominent MRI marker.¹ Many studies have shown an association between WMH and cortical thinning.^{3–5} However, the mechanism behind this association, as well as the tissue composition changes underpinning the decreased cortical thickness, are complex and poorly understood.

Secondary neurodegeneration has been proposed as a potential mechanism through which WMH may contribute to thinning of the regional cortex connected to WMH, thereby influencing the clinical status of SVD.² Studies in other subcortical ischaemic lesions, such as incident lacunes and subcortical infarcts, have shown that regional cortical thinning occurred in areas connected to the initial lesion as a result of degeneration of the connecting white matter tracts, providing evidence for secondary neurodegeneration.^{6,7} In WMH, this mechanism was also partly supported by the Mayer et al.⁸ study, which examined the association between WMH connectivity and cortical thickness. Specifically, the probabilities that WMH and the cortex are connected through white matter tracts, defined as WMH connectivity, showed a negative association with cortical thickness in their study. However, this study was conducted on a community-based population and did not assess the link between reduced cortical thickness and the microstructural damage of the white matter tracts connecting WMH and cortex. These limitations constrain the generalizability of their findings in the SVD population and weaken the evidence supporting the proposed mechanism.

In addition to cortical thinning, other tissue changes in the WMH-connected cortex may occur, including changes in the myelin density and iron deposition. Quantitative MRI (qMRI), such as quantitative R1 ($1/T_1$) maps, quantitative R2* ($1/T_2^*$) maps and quantitative susceptibility maps (QSM), could provide specific indices of *in vivo* tissue composition.⁹ Previous combined histopathology-MRI studies have demonstrated that the R1 value is mainly positively correlated with myelin¹⁰; the R2* value is positively correlated with both myelin and iron¹¹; and the susceptibility value is mainly positively correlated with iron and negatively correlated with myelin.¹² Therefore, the combination of R1, R2* and susceptibility indexes allows us to accurately probe the myelin density

and iron deposition in the cortical tissue. So far, to the best of our knowledge, no study has *in vivo* measured cortical myelin and iron in regions connected to WMH using the combination of quantitative R1, R2* maps and QSM in SVD.

The goal of this study was to employ a multimodal neuroimaging approach to systematically assess the cortical abnormalities in the WMH-connected regional cortex, as well as their associations with microstructural damage of the connecting white matter tracts in SVD patients. We hypothesized that measures of thickness, myelin and iron in the cortical regions connected to WMH are related to the microstructural integrity of the white matter tracts connecting the WMH and the cortex. To test our hypothesis, we used a range of advanced MRI methodologies, including high-resolution T₁-maps, quantitative R1, R2*, susceptibility maps and diffusion-weighted images (DWI) for probabilistic tractography, to specifically measure the cortical thickness, myelin content and iron deposition in the WMH-connected regional cortex. We tested the relations between these measures in the WMH-connected cortical regions and the mean diffusivity (MD) values of the connecting white matter tracts and related the effects of these measures in the WMH-connected cortical regions to cognitive performance.

Materials and methods

Study population

Data were derived from the Radboud University Nijmegen Diffusion tensor and Magnetic resonance imaging Cohort (RUN DMC) study, which is an ongoing prospective study that aims to investigate the causes and clinical consequences of sporadic SVD. Detailed information on the RUN DMC study has been described previously.¹³ In brief, the participants were included in 2006 based on the following criteria: (i) age between 50 and 85 years; (ii) cerebral SVD on MRI (defined as WMH or lacunes); and (iii) cognitive or motor symptoms that could be attributed to SVD. After the baseline data collection, follow-ups were conducted in 2011, 2015 and 2020. We included 230 participants who participated in the third follow-up assessment (2020), based on the availability of Magnetization Prepared 2 Rapid Acquisition Gradient Echoes (MP2RAGE), multi-echo gradient echo (GRE) and multi-shell DWI sequences to perform a cross-sectional analysis. Of the 230 participants, 17 participants were excluded due to the lack of required MRI scans ($n = 7$), low quality of MRI images ($n = 2$), and obvious head movements ($n = 8$) (Supplementary Fig. 1). The study was

approved by the Medical Review Ethics Committee Region Arnhem-Nijmegen, and written informed consent was obtained from all participants.

Neuropsychological assessment

All participants underwent a detailed cognitive assessment. For this study, we used cognitive data covering three cognitive domains: processing speed, executive function, and memory. The raw scores of each cognitive test were standardized as z-scores and then used to compute a compound score for each cognitive domain. Details of these cognitive tests and the calculation of compound scores per cognitive domain are provided in [Supplementary Table 1](#).

MRI acquisition

Participants underwent MRI scanning on a 3 T MRI scanner (MAGNETOM Prisma; Siemens Healthineers) with a 32-channel head coil, including the following sequences: MP2RAGE to construct robust T₁-weighted (T₁W) image and quantitative R1 maps, 3D multi-echo GRE providing magnitude and phase images to create susceptibility weighted image (SWI), R2* (1/T₂^{*}) maps and QSM, 3D fluid-attenuated inversion recovery (FLAIR) image and multi-shell DWI. Detailed parameters for each sequence were provided in the [Supplementary material](#) and described previously.¹³

WMH segmentation

We used a validated 3D U-net deep learning algorithm to automatically segment WMH on registered and bias-corrected T₁ and FLAIR images.¹⁴ All segmented WMH masks were visually inspected. The lacunes located within or at the edge of WMH were excluded from the WMH mask. T₁W images were segmented into grey matter, white matter, and CSF using unified segmentation from the SPM12 toolbox. To avoid misclassifying WMH as grey matter, these segmented grey matter, white matter and CSF images were corrected using the WMH mask. The intracranial volume (ICV) was calculated as the sum of the grey matter, white matter and CSF volumes. WMH volumes were corrected for the ICV.

We performed visual assessments of SVD markers (WMH, lacunes and CMBs) on MRI in accordance with the Standards for Reporting Vascular changes on neuroimaging (STRIVE).¹ Given the absence of perivascular space (PVS) information in our cohort, we did not include PVS in the SVD assessment. WMH was scored using a modified Fazekas scale (mild WMH: Fazekas score 0–1, moderate WMH: Fazekas score 2, severe WMH: Fazekas score 3).¹⁵ Subsequently, a simple SVD score consisting of WMH, lacunes and CMBs was generated to assess the total SVD burden.¹⁶ In this simple SVD score, 1 point was respectively assigned for the WMH Fazekas score ≥ 2 , the number of lacunes ≥ 3 , the presence of CMBs, as described in a previous study.^{16,17}

Diffusion MRI processing

Multi-shell diffusion MRI data were preprocessed for denoising and Gibbs artefact removal using tools from MRtrix 3.0 (<http://www.mrtrix.org>) and subsequently corrected for head motion, eddy currents-induced distortions, susceptibility-induced distortions (topup), intensity bias using the Functional Magnetic Resonance Imaging of the Brain Software Library (FSL; v6.0.1) and the Advanced Normalization Tools (ANTs, v 2.1.0).^{18–22} Next, we used the Bedpostx function within FSL to estimate the voxel-wise multi-

fibre directions based on the ball-and-two-sticks model.²³ Subsequently, tensor fit for the processed diffusion image (only $b = 0$ and $b = 1000$ s/mm² image) was executed using the dtfit function within FSL to produce the fractional anisotropy (FA) and MD images for each participant.

Identification of connected cortex

Probabilistic tractography was performed using the probtrackx2 function within FSL software with the default parameters. WMH mask was employed as the seed mask and the white matter–grey matter boundary derived from Freesurfer (version 7.1.0) as the target mask, producing the ‘fdt_path’ images. In the cortical part of the ‘fdt_path’ image, each voxel value represents the numbers of streamlines connecting cortex and WMH. Subsequently, voxel values in cortical part of the ‘fdt_path’ image were normalized by dividing the total number of streamlines sent out from the seed masks (5000 times per voxel), resulting in a probability map of the cortex connected to WMH. This map was further thresholded at three levels (low, medium and high), as described in the [Supplementary material](#) and previous studies.^{6,7} Lower connectivity levels are more susceptible to noise and may lead to false-positive tracts, whereas higher levels are more specific but might eliminate subordinate connectivity. It is crucial to emphasize that the term ‘connectivity level’ in our study refers solely to the connectivity profile of the cortex (i.e. the connectivity probability to WMH), and does not function as a surrogate marker for white matter microstructural integrity. The cortical regions connected by the tracts were identified as WMH-connected regions. Cortex outside the connected region was defined as WMH-unconnected regions and employed as a control representing the global tissue composition abnormalities unrelated to the WMH ([Fig. 1A](#)).^{6,7} Details are provided in the [Supplementary material](#).

Cortical surface reconstruction and cortical thickness analysis

MP2RAGE images were processed to create the robust T₁W image, using a homemade MATLAB (R2016b; MathWorks, Natick, MA) script,²⁴ which has the advantage of combining the unbiased tissue contrast, while enabling robust and reproducible tissue segmentation.²⁵ The robust T₁W image was fed into the standard ‘recon-all’ processing pipeline within Freesurfer to reconstruct the cortical surface and estimate cortical thickness. The resulting CSF–grey matter boundary (pial surface) and grey matter–white matter boundary (white matter surface) were visually inspected to avoid obvious reconstruction errors. Cortical thickness was measured as the distance between the pial surface and the white matter surface. Notably, given the non-uniform distribution of cortical thickness across the brain regions and the certain connectivity patterns of the WMH to the cortex,^{8,26} it will be hard to attribute any potential thinner cortical thickness detected in the WMH-connected regions to the remote effects of WMH or the interregional differences of cortical thickness. To minimize this effect, we calculated the mean cortical thickness of each brain region using the Desikan–Killiany atlas, which parcellates the cortex into 68 regions based on the morphological features.²⁷ We then normalized the interregional differences by dividing the value of each vertex in the cortical thickness map by the average cortical thickness of the corresponding cortical region of the study population ([Fig. 1C](#) and [Supplementary Fig. 2](#)). The normalized cortical thickness map was subsequently smoothed to improve the signal-to-noise ratio.

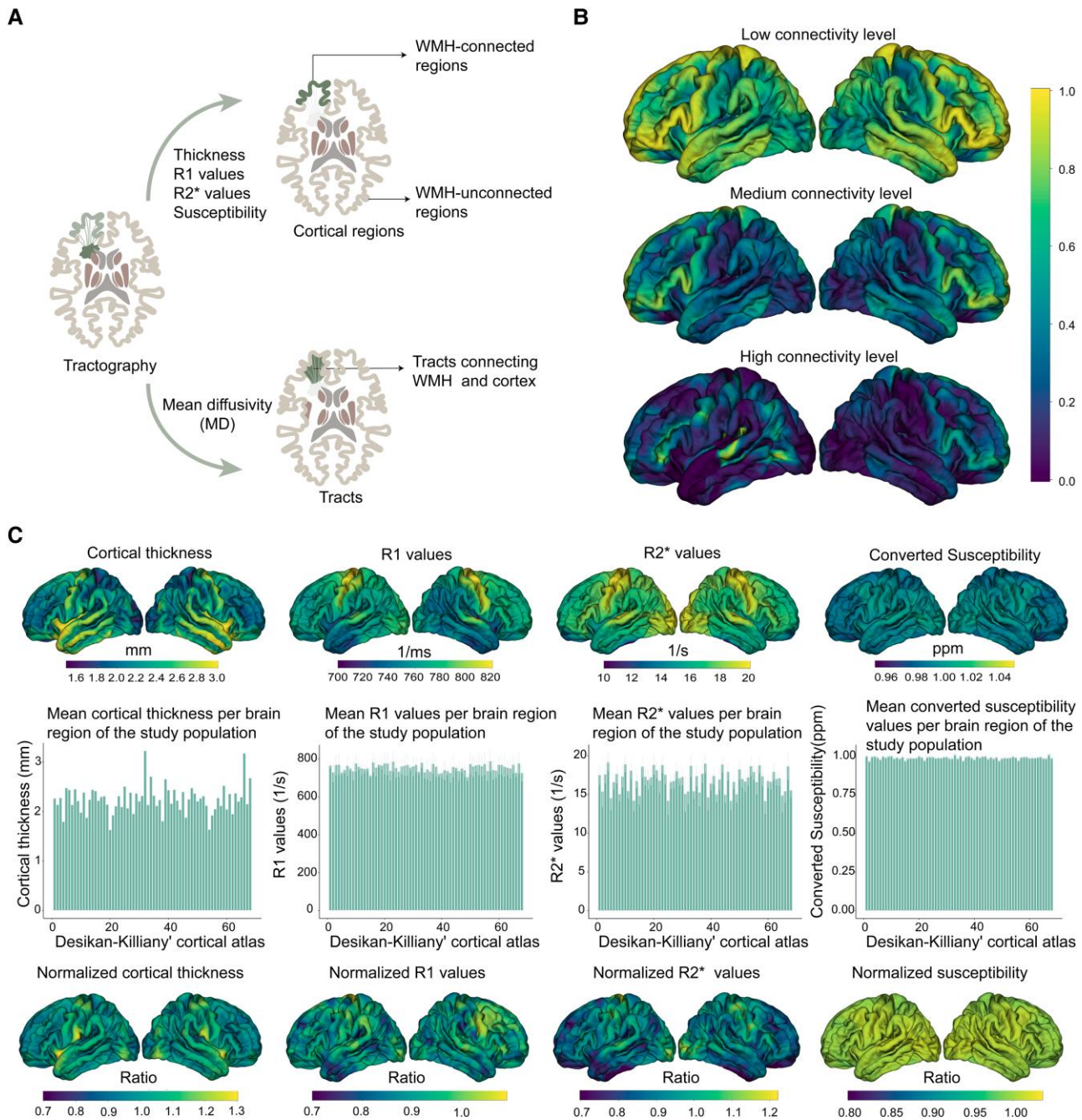


Figure 1 Study design and methods. (A) Probabilistic tractography was performed from white matter hyperintensities (WMH) to the white/grey matter boundary to determine the WMH-connected regions (dark green colour), the WMH-unconnected regions (beige colour) and the connecting white matter tracts (light green colour). (B) The cortical terminations of the connecting white matter tracts were projected to the 'fsaverage' surface template and then averaged across the study population, which represents the connectivity probability originating from WMH. Colour bars indicate the vertex-wise probabilities of the regions connected to the WMH at different threshold levels. (C) Correction for the interregional differences of cortical thickness, R1, R2* susceptibility values at the vertex level. The *top row* shows the averaged cortical thickness, R1, R2* and susceptibility map of the study population; the *middle row* illustrates the different brain regions having a different cortical thickness, R1, R2* and susceptibility values; and the *bottom row* shows the interregional differences after correction by dividing the value of each vertex in cortical thickness/R1/R2*/susceptibility maps by the mean values of the thickness/R1/R2*/susceptibility on the corresponding brain regions of the study population.

The smooth size was set at a 10 mm full-width at half-maximum (FWHM) Gaussian kernel,²⁸ as larger smoothing levels reduce the spatial resolution of surface-based cortical measurements.²⁹ Finally, the mean cortical thickness in the WMH-connected and WMH-unconnected regions was calculated from the normalized-smoothed cortical thickness map.

Surface-based R1 mapping analysis

MP2RAGE images were processed to obtain the quantitative T_1 map using an in-house MATLAB script.³⁰ The quantitative R1 map was created by taking the reciprocal of the T_1 map and scaling that in mHz (ms^{-1}). The R1 map and the robust T_1 image are intrinsically

aligned since they are from the same data (i.e. MP2RAGE image). Next, the R1 map was registered to the 'fsaverage' surface template and sampled along the cortex at the 50% depth from the pial surface to the white matter surface. Resampled cortical R1 maps were visually checked. Given that myelination is known to differ across brain regions,³¹ similar steps to the cortical thickness described above were performed to normalize the interregional differences of R1 (Fig. 1C). The normalized R1 map was then smoothed using a 10 mm FWHM Gaussian kernel and subsequently used to calculate the mean R1 values in the WMH-connected and WMH-unconnected regions.

Surface-based R2* mapping analysis

R2* map was obtained from the multi-echo GRE images, by approximating the integration of the magnitude decay using a closed-form solution based on the trapezoidal rule. This step was achieved using an in-house MATLAB toolbox (<https://github.com/kschan0214/r2starmapping>).³² The R2* map was registered to the corresponding robust T₁W image using 'bregister' function within Freesurfer.³³ Given that previous studies have shown that the values of R2* are typically 15 s⁻¹ for grey matter,³⁴ exceedingly low for CSF and ~30 s⁻¹ for white matter,¹¹ a threshold range from 5 s⁻¹ to 30 s⁻¹ was therefore applied in the R2* map to reduce the partial volume effects from white matter and CSF, as described in the previously study.³⁵ Then, following the similar processing steps described in the above R1 mapping analysis, the R2* map was then registered to the 'fsaverage' surface template, sampled along the cortex, normalized for the interregional differences, smoothed using a 10 mm FWHM Gaussian kernel and finally used to calculate the mean R2* values in the WMH-connected and WMH-unconnected regions.

Surface-based susceptibility mapping analysis

QSM was reconstructed from the multi-echo GRE images using the SEPIA toolbox.³⁶ The reconstruction process included: removing non-brain tissue, the combination of multi-echo phases, phase unwrapping, the background magnetic field removal and the calculation of susceptibility values using CSF as a reference region.^{37–40} QSM was then registered to the corresponding robust T₁W image, and then to the 'fsaverage' surface template, sampled along the cortex, as described in the above R2* map analysis. Of note, the cortical susceptibility included both positive and negative values. We, therefore, took the exponentials of the value of each vertex in the cortical susceptibility map and the exponentials of the average susceptibility of the 68 cortical regions of the study population to keep all values >0, which we termed 'converted susceptibility' ($\chi_{conv} = \exp(\chi)$). Next, the value of each vertex in the converted cortical susceptibility map was divided by the average converted susceptibility values of the corresponding cortical region to normalize for the interregional differences (Fig. 1C) resulting in a region-normalized QSM map. Lastly, the normalized QSM map was smoothed using a 10 mm FWHM Gaussian kernel and then used to calculate the mean susceptibility values in the WMH-connected and WMH-unconnected regions.

Microstructural integrity of the connecting white matter tracts

The connectivity map obtained from the probability tractography above was normalized by dividing the total number of streamlined samples and then thresholded at 2×10^{-4} to achieve the best balance between removing potentially noisy fibre tracts and minimizing any false negative pathways.⁴¹ The thresholded tracts were visually inspected to ensure their accuracy and specificity. Then,

mean MD values for the tracts connecting WMH and the cortex were extracted, and were used as a proxy of white matter microstructural integrity. The MD index was chosen over other diffusion metrics because it is less affected by the crossing fibres and has shown the strongest association with cognitive impairments in SVD.^{42,43}

Statistical analyses

Continuous variables were tested for normality distribution using the Anderson-Darling method and described by mean (standard deviation, SD) or median (interquartile ranges, IQRs), according to their distribution.

To evaluate cortical abnormalities in the WMH-connected regional cortex, we first compared the four cortical metrics (i.e. cortical thickness, R1, R2* and susceptibility values) of WMH-connected regions with those of their corresponding WMH-unconnected regions at three connectivity levels using paired t-tests. Next, we compared the four cortical metrics of WMH-connected regions across three connectivity levels (i.e. low level versus medium level, low level versus high level, medium level versus high level) using three times paired t-tests. We employed three separate paired t-tests instead of analysis of covariance (ANCOVA), because our focus was on pairwise comparisons between cortical metrics at different connectivity levels rather than determining if there is an overall difference among the three connectivity levels.

To investigate the relations between microstructural damage of the connecting white matter tract and the cortical abnormalities of the WMH-connected regions, we employed linear regression analyses. Linear regression models were established using the mean MD values of the connecting white matter tracts as the main independent variables and all cortical metrics (i.e. cortical thickness, R1, R2* and susceptibility values) of WMH-connected regions in three connectivity levels as the dependent variables. Adjustments were made for age, sex and the areas of WMH-connected regions. The inclusion of the areas of WMH-connected regions in the model was essential due to its variability among participants, which may subsequently impact the calculation of the mean values of the cortical metrics. In addition, given that previous studies have demonstrated an association between WMH volumes and cortical thickness,^{3–5} we also performed linear regression analyses to test the relation between WMH volumes and the cortical metrics of the WMH-connected regions, using the same covariates.

To link the cortical abnormalities of WMH-connected region with the cognitive performance, we employed linear regression models. Each cortical metric of the WMH-connected regions at each connectivity level was employed as the independent variable and cognitive score in each domain (i.e. processing speed, executive function and memory) as the dependent variable. To minimize potential confounding effects on cognitive function, we employed two models with different adjustments. Model 1 included age, years of education, areas of WMH-connected regions, WMH volumes and corresponding cortical metrics of WMH-unconnected regions. Model 2 included the mean MD values of the connecting white matter tracts as an additional adjustment based on Model 1. In these linear regression models, WMH volumes and the mean MD values of the connecting white matter tracts were included as covariates due to their potential effects on cognitive function in SVD.^{44,45} The cortical metrics of WMH-unconnected regions were included as control for the global tissue composition abnormalities unrelated to WMH, such as normal ageing and comorbid Alzheimer's disease pathologies, as included in previous studies.^{6,7}

Furthermore, to test if the abnormalities of WMH-connected regions mediated the effects of microstructural damage of the connecting white matter tract on cognitive performance, we employed structural equation model (SEM) using the 'lavaan' package in R. Specifically, we first assessed two latent variables, separately representing global cortical abnormalities of WMH-connected and WMH-unconnected regions, using confirmatory factor analysis (CFA). Following this, we performed mediation analysis with the mean MD values of the connecting white matter tract as the initial variable, the latent variable representing the global cortical abnormalities of the WMH-connected regions as the mediator, and processing speed as the outcome variable. We adjusted for age, years of education, areas of WMH-connected regions, WMH volumes, and global cortical abnormalities in WMH-unconnected region in the mediation analysis. 10 000 bootstrapping samples were used to estimate the 95% confidence interval (CI) and determine statistical significance. Note that the CFA and mediation analyses were only performed at the high connectivity level, as the cortical abnormalities of the WMH-connected regions at this level were the most representative. Processing speed was selected as the only outcome variable based on the results of linear regression analyses between cortical abnormalities in WMH-connected regions and cognitive performance described earlier.

For group comparisons, outliers were identified as values out of the $1.5 \times$ IQRs and removed. For all linear regression models, the dependent variables that did not meet a normal distribution were transformed using the Yeo-Johnson approach to approximate a normal distribution,⁴⁶ and the outliers with a Cook's distance four times greater than the group mean were discarded to prevent outlier bias.⁴⁷ Multicollinearity was also assessed in all linear regression models using variance inflation factors (VIFs), with values of VIFs >10 indicating strong multicollinearity.⁴⁸ For CFA model, the comparative fit index (CFI), root mean square error of approximation (RMSEA), and standardized root mean residual (SRMR) were employed as the indicators of model fit.⁴⁹ An acceptable model fit was determined by CFI values >0.90 , RMSEA values <0.08 , and SRMR values <0.08 .⁴⁹

All statistical analyses were performed using R software (version 4.1.1) and the significance level was set at a two-tailed P -value <0.05 . The Hommel-Hochberg method was employed to perform the correction for multiple comparisons.⁵⁰

Sensitivity analyses

First, to confirm specific relations between the cortical measures of WMH-connected regions and the microstructural damage of the connecting white matter tracts or the WMH volumes, we performed linear regression analyses between the mean MD values of the connecting white matter tracts and the four cortical metrics of WMH-unconnected regions, as well as between WMH volumes and the four cortical metrics of WMH-unconnected regions.

Second, to address the potential partial volume effects for R1, R2* and susceptibility values in cortical regions with cortical thinning, we retested the group differences of R1, R2* and susceptibility values between the WMH-connected and WMH-unconnected regions at three connectivity levels and the group differences of R1, R2* and susceptibility values of the WMH-connected regions across three connectivity levels using ANCOVA, while adjusting for cortical thickness. We also retested the relations between the WMH volumes/mean MD values of the connecting tracts and the R1, R2* and susceptibility values of WMH-connected regions, while additionally adjusting for the cortical thickness of WMH-connected regions.

Results

A total of 213 participants were included in the present study, with a median age of 73 years (IQR, 69–79), and 95 were female (44.6%). Detailed information on demographic data, cognitive function and neuroimaging characteristics were provided in [Table 1](#) and [Supplementary Table 2](#).

Identification of connected cortex

The cortical regions connected to WMH as determined by probabilistic tractography at three connectivity levels were averaged across all participants and visualized on the 'fsaverage' surface. As shown in [Fig. 1B](#), higher connectivity probabilities with WMH were observed in the frontal and occipital regions at all three connectivity levels. The Desikan-Killiany atlas was applied to the probability map to identify the connectivity probabilities of each brain region at three connectivity levels. For the high connectivity level, the top-five ranking of cortical regions with higher connectivity probabilities to WMH were frontal pole, pars triangularis, pars opercularis, superior frontal and pericalcarine ([Supplementary Table 3](#)).

Cortical thickness, R1, R2* and susceptibility in the connected regions

Compared with the WMH-unconnected regions, the cortical thickness, R1, R2* and susceptibility of WMH-connected regions showed significantly lower values at all connectivity levels ($P_{corrected} < 0.001$, [Figs 2–5](#)). The comparisons between the three connectivity levels showed that the WMH-connected regions with higher connectivity levels had more pronounced lower cortical thickness, R1, R2* and susceptibility values ($P_{corrected} < 0.001$, [Figs 2–5](#)).

Higher WMH volumes were related to lower cortical thickness of the WMH-connected regions at the low ($\beta = -0.25$, $P_{corrected} = 0.006$) and medium ($\beta = -0.23$, $P_{corrected} = 0.046$) connectivity levels ([Supplementary Table 4](#)); higher MD values of the connecting white

Table 1 Demographic, clinical and imaging characteristics of the study cohort

	n = 213
Demographic	
Age, years, median (IQR)	73.0 (69.0–79.0)
Female, n (%)	95 (44.6%)
Education, years, median (IQR)	10.0 (10.0–15.0)
Vascular risk factors	
Hypertension, n (%)	139 (65.3%)
Diabetes, n (%)	29 (13.6%)
Hypercholesterolaemia, n (%)	114 (53.5%)
Smoking history, n (%)	136 (63.8%)
Cognition function	
Processing speed, median (IQR)	0.3 (–0.9–1.2)
Executive function, median (IQR)	0.1 (–0.3–0.5)
Memory, median (IQR)	–0.1 (–1.4–1.1)
SVD markers	
Simple SVD score, median (IQR)	0.0 (0.0–1.0)
WMH volumes, ml, median (IQR)	4.1 (1.81–10.7)
Normalized WMH, %, median (IQR)	0.3 (0.1–0.7)
Lacunae, n (%)	54 (25.4%)
CMBs, n (%)	79 (37.1%)
Brain volume, ml, mean (SD)	1084.8 (116.6)

CMBs = cerebral microbleeds; IQR = interquartile range; SD = standard deviation; SVD = small vessel disease; WMH = white matter hyperintensities.

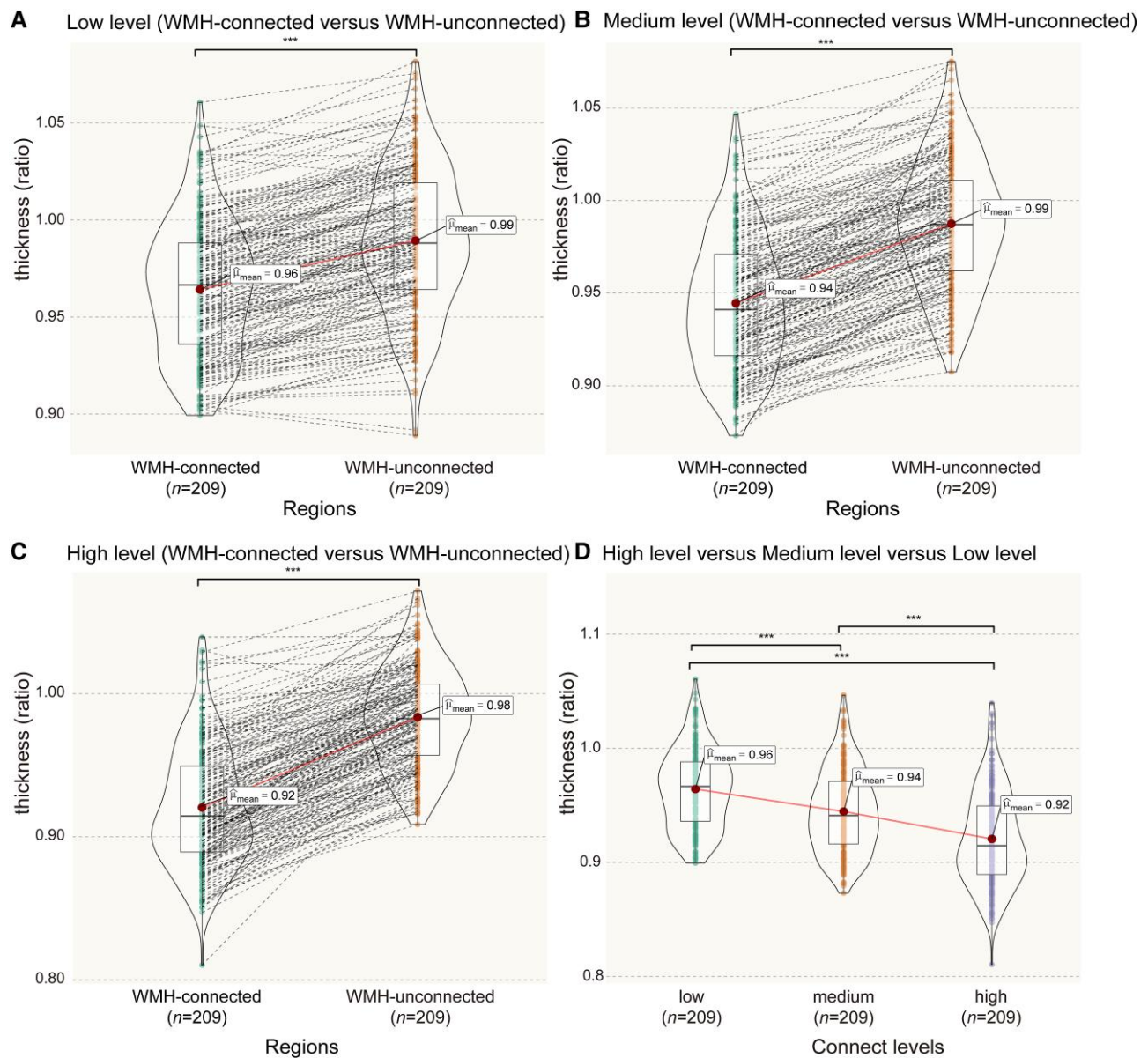


Figure 2 Comparison of cortical thickness between WMH-connected regions and WMH-unconnected regions, and between different connectivity levels. Four participants were identified as outliers, resulting in 209 participants included. (A–C) Compared with the WMH-unconnected regions, the cortical thickness in the WMH-connected regions showed significant decreases at all connectivity levels. (D) The WMH-connected regions with higher connectivity levels had more pronounced lower cortical thickness values. *** $P_{\text{corrected}} < 0.001$. WMH = white matter hyperintensities.

matter tracts were significantly related to lower cortical thickness, lower R1 and R2* values of the WMH-connected regions at three connectivity levels and related to lower susceptibility values of the WMH-connected regions at high connectivity level [$\beta = (-0.389, -0.143)$, $P_{\text{corrected}}$ values < 0.05 , Fig. 6].

Cortical thickness, R1, R2* and susceptibility in the connected regions and cognitive function

Lower scores on processing speed, but not any of the other cognitive domains, were significantly related to lower cortical thickness, lower R1 values, lower R2* values and lower susceptibility values of the WMH-connected regions at three connectivity levels (Table 2). After additionally adjusting for the MD values of the connecting white matter tracts (Model 2): the relations between processing

speed and R1, R2* values of the WMH-connected regions at three connectivity levels, and the relations between processing speed and susceptibility values of the WMH-connected regions at the medium and low connectivity levels remained significant; the relations between processing speed and cortical thickness of the WMH-connected regions and the relation between the processing speed and susceptibility values of the WMH-connected regions at high connectivity level were not significant (Supplementary Table 5).

Two latent variables were separately used to assess the global cortical abnormalities of the WMH-connected regions or the WMH-unconnected regions; both showed great model fit (Supplementary Table 6). The mediation analysis showed that the global cortical abnormalities of WMH-connected regions significantly mediated the relations between the MD values of the

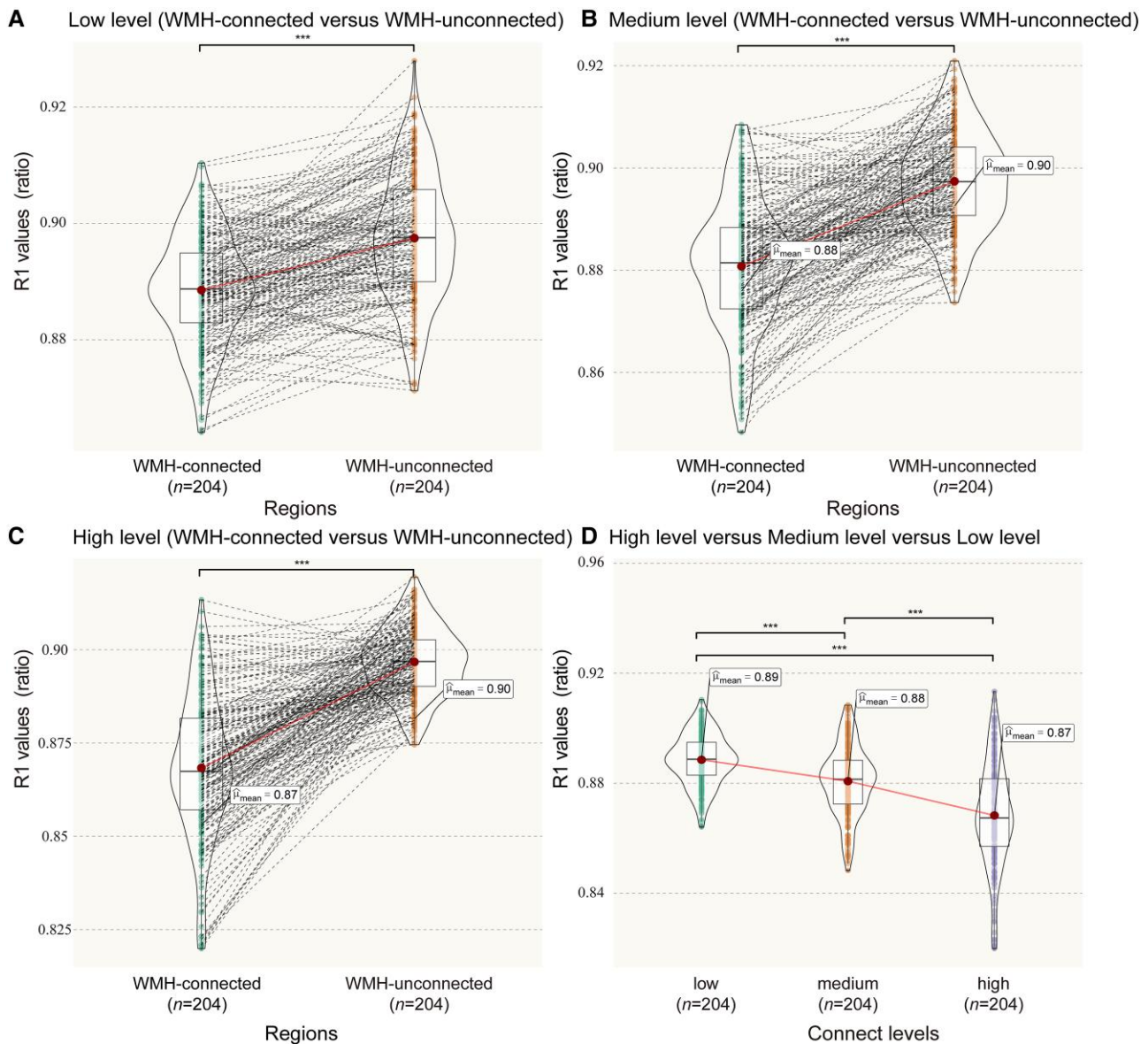


Figure 3 Comparison of R1 values between different WMH-connected regions and WMH-unconnected regions, and between different connectivity levels. Nine participants were identified as outliers, resulting in 204 participants included. (A–C) Compared with the WMH-unconnected regions, the R1 values in the WMH-connected regions showed significant decreases at all connectivity levels. (D) The WMH-connected regions with higher connectivity levels had more pronounced lower R1 values. $***P_{corrected} < 0.001$. WMH = white matter hyperintensities.

connecting white matter tracts and the processing speed (indirect effect = -0.09 , P -values = 0.011 , direct effect = -0.04 , P -values = 0.595 , [Supplementary Fig. 3](#)).

Sensitivity analyses

In contrast to the WMH-connected regions, the mean MD values of the connecting white matter tracts were not related to the cortical thickness, R1 and R2* values of the WMH-unconnected regions across three connectivity levels. However, at medium and high connectivity levels, higher MD values of the connecting white matter tracts were significantly correlated with higher susceptibility values of the WMH-unconnected regions ([Supplementary Table 7](#)). Furthermore, at the low connectivity level, higher WMH volumes were related to reduced cortical thickness of the WMH-unconnected regions ([Supplementary Table 8](#)).

After adjusting for cortical thickness, the results for group differences in R1, R2* and susceptibility values between the WMH-connected and WMH-unconnected regions and between the WMH-connected regions across three connectivity levels and for the relations between the WMH volumes/mean MD values of the connecting tracts and the R1, R2* and susceptibility values of WMH-connected regions remained largely unchanged ([Supplementary Fig. 4](#) and [Supplementary Table 9](#)).

Discussion

In the present study, we employed a multimodal neuroimaging study to systematically assess the cortical abnormalities connected to WMH in SVD. We found that (i) white matter tracts passing through WMH showed a specific connectivity pattern to the cortex, with

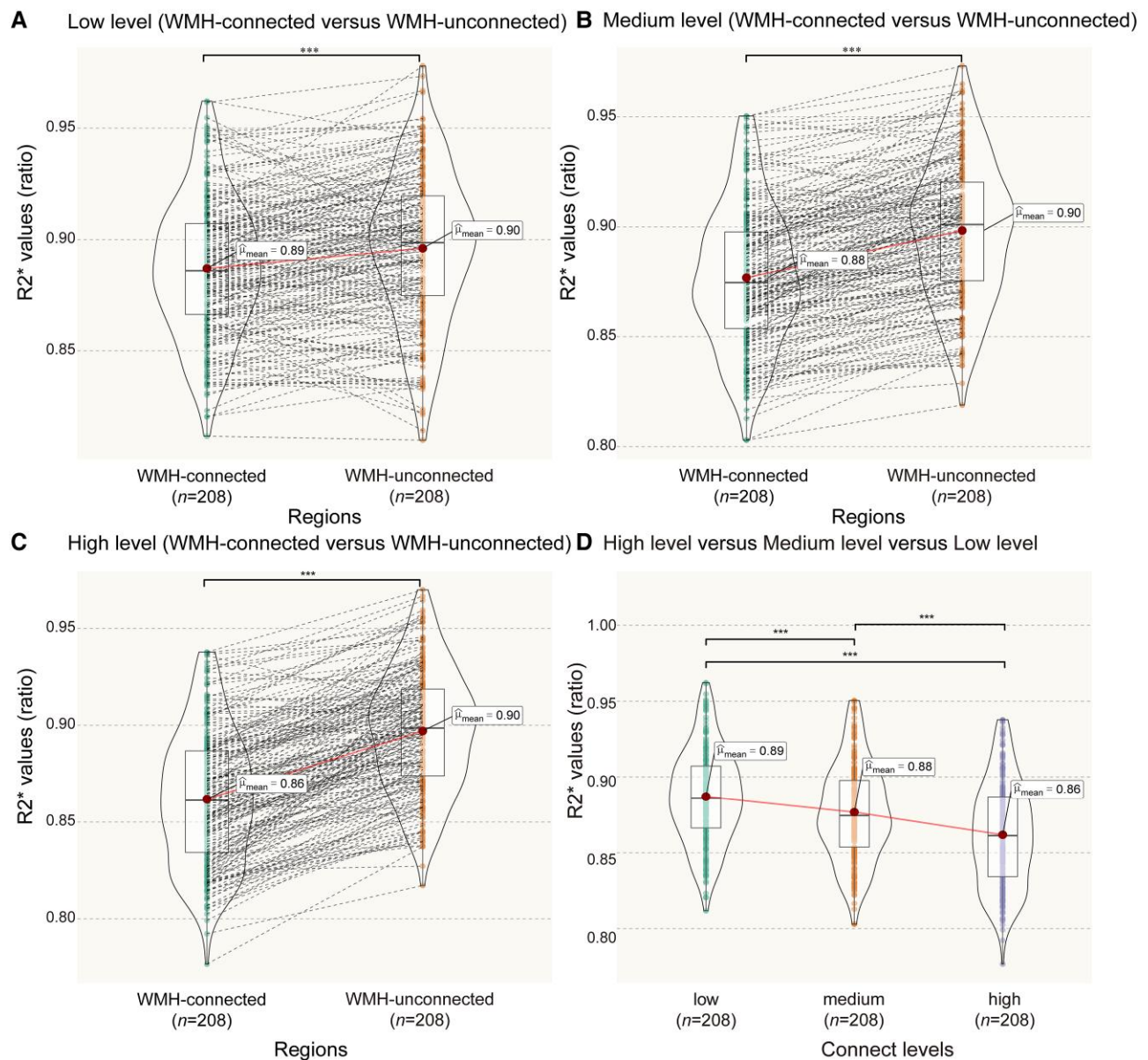


Figure 4 Comparison of R2* values between WMH-connected regions and WMH-unconnected regions, and between different connectivity levels. Five participants were identified as outliers, resulting in 208 participants included. (A–C) Compared with the WMH-unconnected regions, the R2* values in the WMH-connected regions showed significant decreases at three connectivity levels. (D) The WMH-connected regions with higher connectivity levels had more pronounced decreases in R2* values. *** $P_{corrected} < 0.001$. WMH = white matter hyperintensities.

higher connectivity probabilities to the frontal and occipital regions; (ii) compared to WMH-unconnected cortical regions, WMH-connected cortical regions showed significantly lower thickness, R1, R2* and susceptibility values; (iii) higher MD of the connecting white matter tracts were related to lower cortical thickness, R1, R2* and susceptibility values in the WMH-connected regions; (iv) lower cortical thickness, R1, R2* and susceptibility values in the WMH-connected regions were significantly and specifically related to lower scores on processing speed; and (v) these cortical abnormalities of the WMH-connected regions mediated the relations between MD values of the connecting white matter tracts and processing speed. Taken together, our results suggest that WMH is related to changes in the connected cortex (e.g. cortical thinning, demyelination and iron loss), most likely through the disruption of connecting white matter tracts. These cortical tissue changes may lead to processing speed

impairment, a key clinical feature of SVD.⁵¹ These findings advance our understanding of the mechanisms of cognitive impairment in SVD.

In our study, WMH displayed a higher connectivity probability to the frontal and occipital regions. This finding corroborates the Mayer *et al.*⁸ study, showing a similar connectivity pattern of WMH to the cortex. Notably, that same employed a different tractography approach (whole-brain tractography) and focused on a community-based population, as opposed to the SVD population in the present study. Nevertheless, our findings confirmed the robustness of the connectivity pattern of WMH (of presumed vascular origin) to the cortex across different tractography methods and populations. However, it is worth noting that WMH resulting from other pathologies, such as in multiple sclerosis or Alzheimer's disease, may have different connectivity patterns,^{52,53} which requires further investigation.

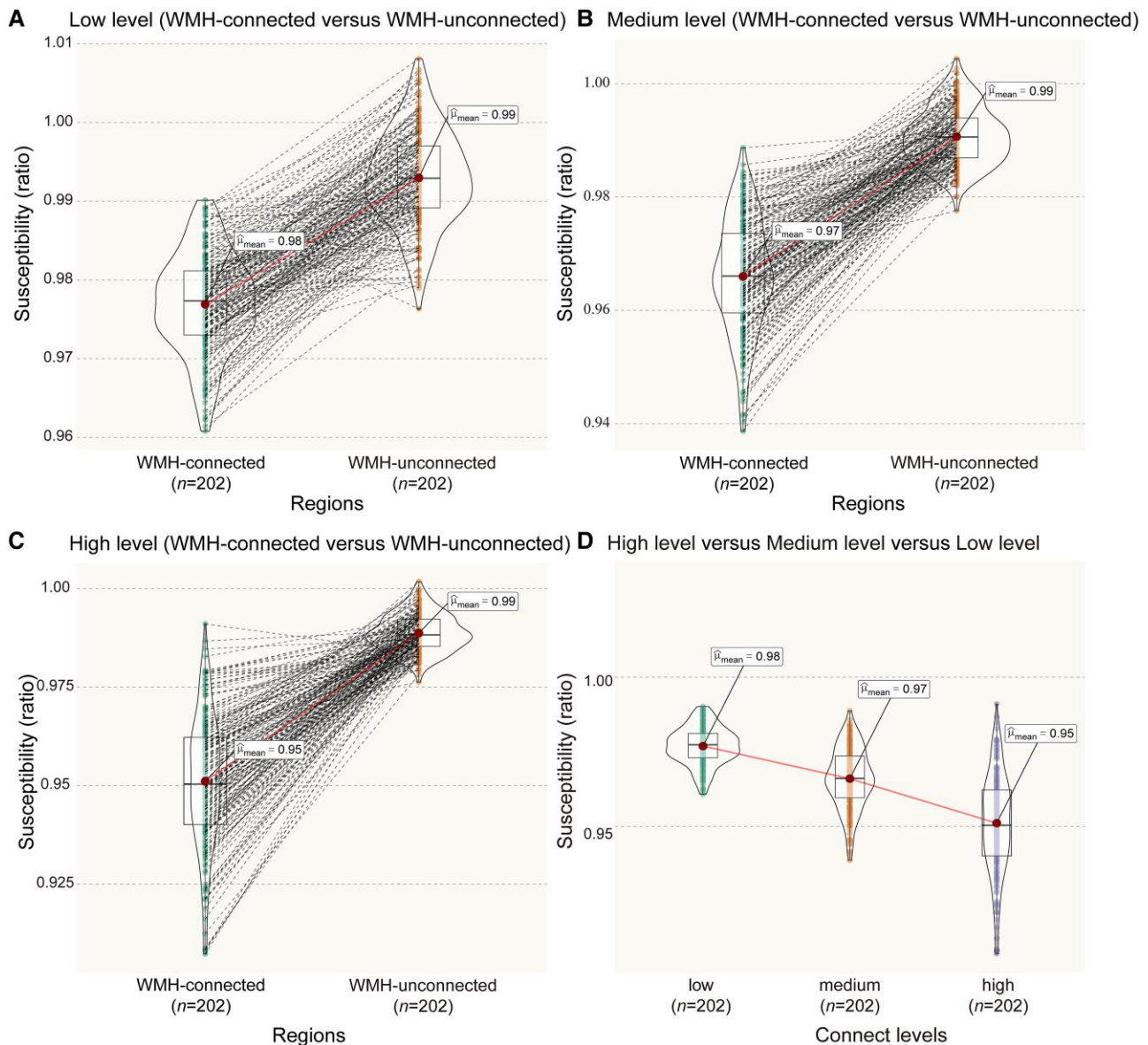


Figure 5 Comparison of susceptibility values between WMH-connected regions and WMH-unconnected regions, and different connectivity levels. Eleven participants were identified as outliers, resulting in 202 participants included. (A–C) Compared with the WMH-unconnected regions, the susceptibility values in the WMH-connected regions showed significant decreases at three connectivity levels. (D) The WMH-connected regions with higher connectivity levels had more pronounced decreases in susceptibility values. *** $P_{\text{corrected}} < 0.001$. WMH = white matter hyperintensities.

We found that compared to WMH-unconnected regions, WMH-connected regions showed a significantly lower cortical thickness. Cortical thinning was more pronounced in cortical regions with a higher probability connected to the WMH. This finding is in line with a previous study, which showed that a higher connectivity probability between WMH and the cortex was associated with a reduced cortical thickness.⁸ Moreover, we found that higher MD values of the connecting white matter tracts were specifically related to lower cortical thickness of WMH-connected regions, but not to that of the WMH-unconnected regions. This pattern of regional cortical thinning linked to the microstructural integrity of connecting tracts strengthens the suggestion that cortical thinning occurs, at least partially, as a result of secondary neurodegeneration of white matter tracts between WMH and the cortex. This mechanism is further substantiated by the finding that subcortical ischaemic lesions could induce regional connected cortical

alterations remote from the lesions through disruption of white matter tracts in studies involving cerebral autosomal dominant arteriopathy with subcortical infarcts and leukoencephalopathy (CADASIL) or stroke participants.^{6,7} In addition, we found that higher WMH volumes were significantly related to lower cortical thickness of WMH-unconnected regions, which may be explained by other cortical pathological processes accompanying WMH, such as cortical microinfarction, increased blood–brain barrier permeability, and inflammation.⁵⁴

Furthermore, we found that, compared to the WMH-unconnected regions, the R1 and R2* values were significantly lower in WMH-connected regions that were associated with higher MD values of the connecting white matter tracts. These findings are suggestive of cortical demyelination of the connected cortex. No studies have previously examined cortical myelination changes in SVD. In multiple sclerosis, however, the demyelination of the cortex is well

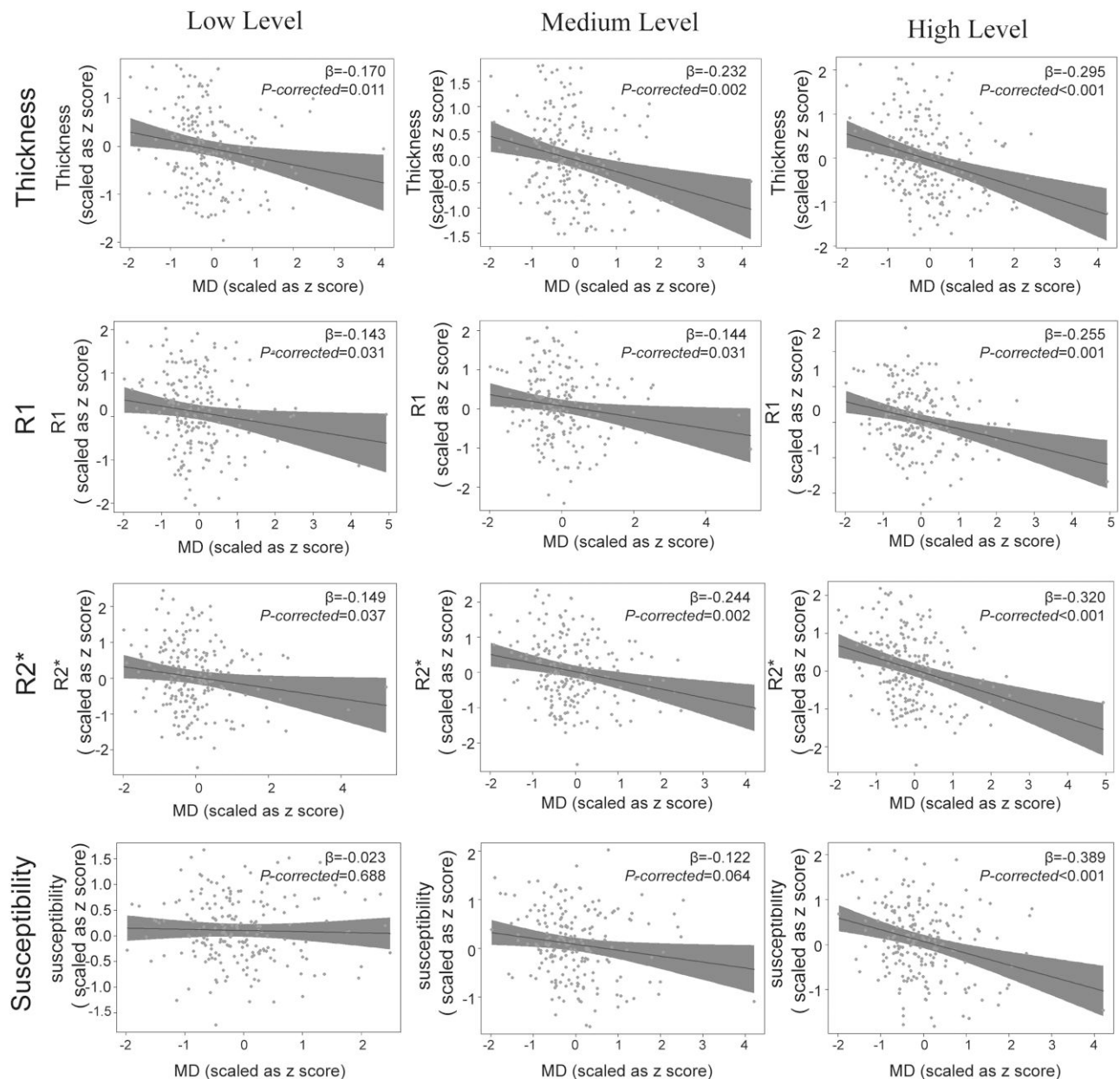


Figure 6 Relations between MD of connecting white matter tracts and the mean thickness, R1 and R2*, susceptibility values of the WMH-connected regions. In the top row, the higher mean diffusivity (MD) of the connecting white matter tracts was related to the lower thickness of the WMH-connected regions at three connectivity levels. In the second row, the higher MD of the connecting white matter tracts was related to lower R1 values of the WMH-connected regions at three connectivity levels. In the third row, the higher MD of the connecting white matter tracts was related to lower R2* values of the WMH-connected regions at three connectivity levels. In the fourth row, the higher MD of the connecting white matter tracts was related to lower susceptibility values of the WMH-connected regions at the high connectivity level; $P_{corrected}$ values represent P-values corrected for multiple comparisons using the Hommel-Hochberg method. WMH = white matter hyperintensities.

established.^{55,56} A longitudinal study in multiple sclerosis reported that microstructural damages of white matter tracts at baseline predicted myelin loss in the connected cortical regions at the 2-year follow-up.⁵⁷ This evidence strengthened our hypothesis that WMH can lead to cortical demyelination through secondary degeneration of the connecting white matter tracts. In addition, it can be speculated that the cortical thinning observed in the WMH-connected region may not solely arise from neuronal loss but also from reduction in myelinated fibres.

We also found decreased susceptibility values in the WMH-connected regions compared with the WMH-unconnected regions.

Given that susceptibility values have demonstrated a predominant positive correlation with iron and a negative correlation with myelin,¹² the decreased susceptibility values observed in the WMH-connected regions strongly indicate iron loss. Similar iron loss in the cortex has been found in multiple sclerosis.^{56,58} Furthermore, multiple sclerosis patients with long disease duration showed decreased iron concentration in the thalamus, whereas those with short disease duration or diagnosed as clinically isolated syndrome did not exhibit such changes.^{59,60} Given that oligodendrocytes store most of the iron and that iron is involved in various metabolic processes,⁶¹ the iron loss during the progression of the

Table 2 Relation between cortical thickness, R1, R2*, and susceptibility values of the WMH-connected regions and cognitive function

	Processing speed		Executive function		Memory	
	β	P-corrected value	β	P-corrected value	β	P-corrected value
Cortical thickness of the WMH-connected regions						
High level	0.20	0.030	-0.07	0.988	-0.02	0.896
Medium level	0.28	0.030	0.02	0.988	0.06	0.896
Low level	0.33	0.030	0.33	0.170	0.08	0.896
R1 of the WMH-connected regions						
High level	0.20	0.006	0.02	0.988	0.01	0.896
Medium level	0.25	0.002	0.06	0.988	0.08	0.896
Low level	0.26	0.006	0.10	0.988	0.10	0.896
R2* of the WMH-connected regions						
High level	0.29	0.006	-0.17	0.459	-0.03	0.896
Medium level	0.43	<0.001	-0.27	0.180	0.04	0.896
Low level	0.42	0.001	-0.23	0.261	0.04	0.896
Susceptibility value of the WMH-connected regions						
High level	0.19	0.024	-0.04	0.988	-0.04	0.896
Medium level	0.23	0.010	0.00	0.988	-0.04	0.896
Low level	0.27	0.010	0.06	0.988	-0.05	0.896

All models were adjusted for age, education years, the areas of white matter hyperintensities (WMH)-connected regions, the WMH volumes, and the cortical changes of the WMH-unconnected regions. P-values were corrected using the Hommel-Hochberg method. P-values in bold represent P-corrected value < 0.05.

disease may signify a reduction in oligodendrocyte density or depletion of iron due to repair of oligodendrocytes.⁵⁹ Studies with long-term follow-up and histology data are required to verify whether iron level of the WMH-connected regions decreases with time in SVD patients.

Besides, we found a positive relationship between susceptibility values of the WMH-unconnected regions and MD values of the connecting white matter tracts, which was unexpected. This finding suggests that there are mechanisms other than secondary degeneration of the connecting white matter tracts that can lead to cortical iron abnormalities in SVD. For example, a previous study found increased R2* values at the site of the acute micro-cortical infarcts,³⁵ and studies in CADASIL reported that an increased blood-brain barrier permeability was associated with increased susceptibility values in the cortex.⁶² Further work is warranted to better understand these observations.

Lastly, we found that decreased thickness R1, R2* and susceptibility values in WMH-connected regions were related to lower scores on processing speed, independent of global tissue composition abnormalities unrelated to WMH. Moreover, these global cortical abnormalities of the WMH-connected regions mediated the relations between microstructural damage of the connecting white matter tract and processing speed. This relation could be explained by a distinctive connectivity pattern of WMH to the cortex and specific tissue changes of WMH-connected regions. Previous studies in SVD have argued that the effects of lesions in the frontal subcortical network are mediated by frontal cortical changes (i.e. cortical thinning) and in combination underlie processing speed deficits.^{63,64} In addition, cortical demyelination and obstructed remyelination (i.e. suggested by iron loss) in the connected cortical regions may also be contributing factors to processing speed deficits in SVD. Myelinating oligodendrocytes contribute to cortical information processing through their dual role of accelerating impulse propagation and supplying metabolic support to the spiking axons.⁶⁵ Our findings, combined with the fact that processing speed is the earliest and the most prominent cognitive domain affected,^{51,66} highlight the significance of cortical pathologies caused by secondary degeneration in determining cognitive deficits in SVD. Interventions targeting the secondary degeneration

of the cortex and the myelin repair might ameliorate the cognitive impairment in SVD.

The strengths of our study include a deeply phenotyped cohort sample of SVD with comprehensive and detailed cognitive data. In addition, we used a state-of-the-art multimodal neuroimaging approach for identification of WMH-connected cortical regions and the *in vivo* cortical histopathological measurements. Furthermore, we corrected the non-uniform distribution of cortical thickness, myelin and iron across brain regions by dividing the thickness, R1, R2* and susceptibility values of each vertex in the cortical maps by the average values of the corresponding metrics of the corresponding cortical region of the study population. This method allowed us to compare changes between different cortical regions (i.e. the WMH-connected regions and unconnected regions) within one subject, thereby excluding cortical changes caused by other factors, such as normal ageing and global brain atrophy. Lastly, we excluded the lacunes located within or at the edge of WMH from the WMH mask, thereby minimizing the potential confounding effects of lacunes on the cortical abnormalities.⁶

Several limitations should be acknowledged. First, the availability of MP2RAGE, multi-echo GRE, and multi-shell DWI images enabled us to comprehensively assess the cortical abnormalities but limited us to only use the third follow-up data from the RUN DMC cohort and to only conduct cross-sectional analyses. Future longitudinal data are needed to test the directionality of the observed relations between the microstructural damage of connecting white matter tracts and cortical measures in the WMH-connected cortex, but also the speculated iron dynamic changes with the disease progression. Second, our cohort lacked age-matched healthy controls. We performed comparisons between changes in WMH-connected regions and WMH-unconnected regions within one subject. This limited the interpretation of our results, since the observed cortical differences between WMH-connected and WMH-unconnected regions may come from the non-uniform distribution of cortical features across brain regions, even though we have minimized this effect through the normalization. Third, in the context of cortical thinning in the WMH-connected regions, the measures of R1, R2* and susceptibility could be more vulnerable to contamination

from CSF or white matter signals (i.e. the increased partial volume effects). To minimize this effect, we applied a threshold range [(5–30)1/s] in the $R2^*$ map to exclude signals from CSF or the white matter. We also repeated the analyses involving $R1$, $R2^*$ and susceptibility values while adjusting for cortical thickness, which did not alter our main findings. Fourth, the tissue composition probed by qMRI are based on the different contributions of various components to the magnetic time and/or susceptibility. Beyond the myelin and iron, $R1$, $R2^*$ and susceptibility values are also affected by other sources, such as the cell density or other trace elements.⁶⁷ Further histopathological and longitudinal studies are required to confirm our results. Lastly, our cohort lacked data regarding enlarged PVS, an emergent and promising MRI marker in SVD.⁶⁸ The assessment of PVS should be included in future SVD studies.

Conclusion

In conclusion, our study demonstrated that the microstructural integrity of white matter tracts passing from WMH is related to regional cortical abnormalities as measured by thickness, $R1$, $R2^*$ and susceptibility values in the connected cortical regions. These findings indicate cortical thinning, demyelination and iron loss in the cortex, which is most likely through the disruption of the connecting white matter tracts, and these cortical abnormalities may contribute to processing speed dysfunction in SVD. These findings highlight the role of secondary degeneration in determining cortical thinning, histopathological changes, and deficits in processing speed and may have implications for finding intervention targets for the treatment of cognitive impairment in SVD by preventing secondary degeneration.

Data availability

The data that support the findings of this study are available from the corresponding author, depending on reasonable request from qualified investigators after permission of the appropriate regulatory bodies.

Funding

This work was supported by China Scholarship Council (No 202106380078 to H.L.), Dutch Brain Foundation personal fellowship [H04-12; F2009(1)-16 to F.-E.d.L.], VIDi innovational grant from The Netherlands Organization for Health Research and Development (ZonMw grant 016.126.351 to F.-E.d.L.), A.M.T. is a junior staff member of the Dutch Heart Foundation (grant number 2016T044).

Competing interests

The authors report no competing interests.

Supplementary material

Supplementary material is available at *Brain* online.

References

1. Wardlaw JM, Smith EE, Biessels GJ, et al. Neuroimaging standards for research into small vessel disease and its contribution to ageing and neurodegeneration. *Lancet Neurol.* 2013;12:822–838.
2. Wardlaw JM, Smith C, Dichgans M. Small vessel disease: Mechanisms and clinical implications. *Lancet Neurol.* 2019;18:684–696.
3. Tuladhar AM, Reid AT, Shumskaya E, et al. Relationship between white matter hyperintensities, cortical thickness, and cognition. *Stroke.* 2015;46:425–432.
4. Lambert C, Sam Narean J, Benjamin P, Zeestraten E, Barrick TR, Markus HS. Characterising the grey matter correlates of leukoaraiosis in cerebral small vessel disease. *NeuroImage Clin.* 2015;9:194–205.
5. Lambert C, Benjamin P, Zeestraten E, Lawrence AJ, Barrick TR, Markus HS. Longitudinal patterns of leukoaraiosis and brain atrophy in symptomatic small vessel disease. *Brain.* 2016; 139(Pt):1136–1151.
6. Duering M, Righart R, Csanadi E, et al. Incident subcortical infarcts induce focal thinning in connected cortical regions. *Neurology.* 2012;79:2025–2028.
7. Duering M, Righart R, Wollenweber FA, Zietemann V, Gesierich B, Dichgans M. Acute infarcts cause focal thinning in remote cortex via degeneration of connecting fiber tracts. *Neurology.* 2015;84:1685–1692.
8. Mayer C, Frey BM, Schlemm E, et al. Linking cortical atrophy to white matter hyperintensities of presumed vascular origin. *J Cereb Blood flow Metab.* 2021;41:1682–1691.
9. van den Brink H, Doubal FN, Duering M. Advanced MRI in cerebral small vessel disease. *Int J Stroke.* 2023;18:28–35.
10. Lutti A, Dick F, Sereno MI, Weiskopf NJN. Using high-resolution quantitative mapping of $R1$ as an index of cortical myelination. *NeuroImage.* 2014;93:176–188.
11. Langkammer C, Krebs N, Goessler W, et al. Quantitative MR imaging of brain iron: A postmortem validation study. *Radiology.* 2010;257:455–462.
12. Langkammer C, Schweser F, Krebs N, et al. Quantitative susceptibility mapping (QSM) as a means to measure brain iron? A post mortem validation study. *NeuroImage.* 2012;62:1593–1599.
13. Cai M, Jacob MA, van Loenen MR, et al. Determinants and temporal dynamics of cerebral small vessel disease: 14-year follow-up. *Stroke.* 2022;53:2789–2798.
14. Shelhamer E, Long J, Darrell T. Fully convolutional networks for semantic segmentation. *IEEE Trans Pattern Anal Mach Intell.* 2017; 39:640–651.
15. Fazekas F, Chawluk JB, Alavi A, Hurtig HI, Zimmerman RA. MR Signal abnormalities at 1.5 T in Alzheimer's dementia and normal aging. *Am J Roentgenol.* 1987;149:351–356.
16. Amin Al Olama A, Wason JMS, Tuladhar AM, et al. Simple MRI score aids prediction of dementia in cerebral small vessel disease. *Neurology.* 2020;94:e1294–e1302.
17. Li H, Cai M, Jacob MA, et al. Dissociable contributions of thalamic-subregions to cognitive impairment in small vessel disease. *Stroke.* 2023;54:1367–1376.
18. Kellner E, Dhital B, Kiselev VG, Reiser M. Gibbs-ringing artifact removal based on local subvoxel-shifts. *Magn Resonan Med.* 2016;76:1574–1581.
19. Veraart J, Novikov DS, Christiaens D, Ades-Aron B, Sijbers J, Fieremans E. Denoising of diffusion MRI using random matrix theory. *NeuroImage.* 2016;142:394–406.
20. Andersson JLR, Sotiropoulos SN. An integrated approach to correction for off-resonance effects and subject movement in diffusion MR imaging. *NeuroImage.* 2016;125:1063–1078.
21. Smith SM, Jenkinson M, Woolrich MW, et al. Advances in functional and structural MR image analysis and implementation as FSL. *NeuroImage.* 2004;23(Suppl 1):S208–S219.

22. Tustison NJ, Avants BB, Cook PA, et al. N4ITK: Improved N3 bias correction. *IEEE Trans Pattern Anal Mach Intell.* 2010;29:1310-1320.
23. Jbabdi S, Sotiropoulos SN, Savio AM, Graña M, Behrens TE. Model-based analysis of multishell diffusion MR data for tractography: How to get over fitting problems. *Magn Resonan Med.* 2012;68:1846-1855.
24. Marques JP, Kober T, Krueger G, van der Zwaag W, Van de Moortele PF, Gruetter R. MP2RAGE, A self bias-field corrected sequence for improved segmentation and T1-mapping at high field. *NeuroImage.* 2010;49:1271-1281.
25. O'Brien KR, Kober T, Hagmann P, et al. Robust T1-weighted structural brain imaging and morphometry at 7T using MP2RAGE. *PLoS One.* 2014;9:e99676.
26. Fukutomi H, Glasser MF, Zhang H, et al. Neurite imaging reveals microstructural variations in human cerebral cortical gray matter. *NeuroImage.* 2018;182:488-499.
27. Desikan RS, Ségonne F, Fischl B, et al. An automated labeling system for subdividing the human cerebral cortex on MRI scans into gyral based regions of interest. *NeuroImage.* 2006;31:968-980.
28. Muthuraman M, Fleischer V, Kroth J, et al. Covarying patterns of white matter lesions and cortical atrophy predict progression in early MS. *Neurol Neuroimmunol Neuroinflamm.* 2020;7(3):e681.
29. Coalson TS, Van Essen DC, Glasser MF. The impact of traditional neuroimaging methods on the spatial localization of cortical areas. *Proc Natal Acad Sci U S A.* 2018;115:E6356.
30. Shams Z, Norris DG, Marques JP. A comparison of in vivo MRI based cortical myelin mapping using T1w/T2w and R1 mapping at 3 T. *PLoS One.* 2019;14:e0218089.
31. Ganzetti M, Wenderoth N, Mantini D. Whole brain myelin mapping using T1- and T2-weighted MR imaging data. *Front Hum Neurosci.* 2014;8:671.
32. Khabipova D, Wiaux Y, Gruetter R, Marques JP. A modulated closed form solution for quantitative susceptibility mapping—a thorough evaluation and comparison to iterative methods based on edge prior knowledge. *NeuroImage.* 2015;107:163-174.
33. Greve DN, Fischl B. Accurate and robust brain image alignment using boundary-based registration. *NeuroImage.* 2009;48:63-72.
34. Weiskopf N, Suckling J, Williams G, et al. Quantitative multi-parameter mapping of R1, PD(*), MT, and R2(*) at 3T: A multi-center validation. *Front Neurosci.* 2013;7:95.
35. Wiegertjes K, Chan KS, Telgte AT, et al. Assessing cortical cerebral microinfarcts on iron-sensitive MRI in cerebral small vessel disease. *J Cereb Blood flow Metab.* 2021;41:3391-3399.
36. Chan KS, Marques JP. SEPIA-Susceptibility mapping pipeline tool for phase images. *NeuroImage.* 2021;227:117611.
37. Smith SM. Fast robust automated brain extraction. *Hum Brain Mapp.* 2002;17:143-155.
38. Karsa A, Shmueli K. SEGUE: A speedy rEgion-growing algorithm for unwrapping estimated phase. *IEEE Transact Med Imaging.* 2019;38:1347-1357.
39. Liu T, Khalidov I, de Rochefort L, et al. A novel background field removal method for MRI using projection onto dipole fields (PDF). *NMR Biomed.* 2011;24:1129-1136.
40. Liu T, Liu J, de Rochefort L, et al. Morphology enabled dipole inversion (MEDI) from a single-angle acquisition: Comparison with COSMOS in human brain imaging. *Magn Resonan Med.* 2011;66:777-783.
41. Brumer I, De Vita E, Ashmore J, Jarosz J, Borri M. Reproducibility of MRI-based white matter tract estimation using multi-fiber probabilistic tractography: Effect of user-defined parameters and regions. *MAGMA.* 2022;35:365-373.
42. Dauguet J, Peled S, Berezovskii V, et al. Comparison of fiber tracts derived from in-vivo DTI tractography with 3D histological neural tract tracer reconstruction on a macaque brain. *NeuroImage.* 2007;37:530-538.
43. van Norden AG, van Uden IWM, de Laat KF, van Dijk EJ, de Leeuw FE. Cognitive function in small vessel disease: The additional value of diffusion tensor imaging to conventional magnetic resonance imaging: The RUN DMC study. *J Alzheimer's Dis.* 2012;32:667-676.
44. Hu HY, Ou YN, Shen XN, et al. White matter hyperintensities and risks of cognitive impairment and dementia: A systematic review and meta-analysis of 36 prospective studies. *Neurosci Biobehav Rev.* 2021;120:16-27.
45. Coenen M, Kuijf HJ, Huenges Wajer IMC, et al. Strategic white matter hyperintensity locations for cognitive impairment: A multicenter lesion-symptom mapping study in 3525 memory clinic patients. *Alzheimer's Dementia.* 2022;19:2420-2432.
46. Yeo IK, Johnson RA. A new family of power transformations to improve normality or symmetry. *Biometrika.* 2000;87:954-959.
47. Cook RDJT. Detection of influential observation in linear regression. *Technometrics.* 1977;19:15-18.
48. Akinwande MO, Dikko HG, Samson AJO. Variance inflation factor: As a condition for the inclusion of suppressor variable (s) in regression analysis. *Open J Stat.* 2015;5:754.
49. Goretzko D, Siemund K, Sterner PJE, Measurement P. Evaluating model fit of measurement models in confirmatory factor analysis. *Educ Psychol Meas.* Published online 2 April 2023. <https://doi.org/10.1177/00131644231163813>
50. Hommel GJB. A stagewise rejective multiple test procedure based on a modified Bonferroni test. *Biometrika.* 1988;75:383-386.
51. Salvadori E, Brambilla M, Maestri G, et al. The clinical profile of cerebral small vessel disease: Toward an evidence-based identification of cognitive markers. *Alzheimer's Dementia.* 2023;19:244-260.
52. Garnier-Crussard A, Cotton F, Krolak-Salmon P, Chételat G. White matter hyperintensities in Alzheimer's disease: Beyond vascular contribution. *Alzheimer's Dement.* 2023;19(8):3738-3748.
53. Brown RB, Traylor M, Burgess S, Sawcer S, Markus HS. Do cerebral small vessel disease and multiple sclerosis share common mechanisms of white matter injury? *Stroke.* 2019;50:1968-1972.
54. Wardlaw JM, Smith C, Dichgans M. Mechanisms of sporadic cerebral small vessel disease: Insights from neuroimaging. *Lancet Neurol.* 2013;12:483-497.
55. Lommers E, Simon J, Reuter G, et al. Multiparameter MRI quantification of microstructural tissue alterations in multiple sclerosis. *NeuroImage Clin.* 2019;23:101879.
56. Mainero C, Louapre C, Govindarajan ST, et al. A gradient in cortical pathology in multiple sclerosis by in vivo quantitative 7 T imaging. *Brain.* 2015;138(Pt):932-945.
57. Bodini B, Chard D, Altmann DR, et al. White and gray matter damage in primary progressive MS: The chicken or the egg? *Neurology.* 2016;86:170-176.
58. Bian W, Tranvinh E, Tourdias T, et al. In vivo 7T MR quantitative susceptibility mapping reveals opposite susceptibility contrast between cortical and white matter lesions in multiple sclerosis. *Am J Neuroradiol.* 2016;37:1808-1815.
59. Schweser F, Raffaini Duarte Martins AL, Hagemeyer J, et al. Mapping of thalamic magnetic susceptibility in multiple sclerosis indicates decreasing iron with disease duration: A proposed mechanistic relationship between inflammation and oligodendrocyte vitality. *NeuroImage.* 2018;167:438-452.
60. Burgetova A, Dusek P, Vaneckova M, et al. Thalamic iron differentiates primary-progressive and relapsing-remitting multiple sclerosis. *Am J Neuroradiol.* 2017;38:1079-1086.
61. Meguro R, Asano Y, Odagiri S, Li C, Shoumura K. Cellular and subcellular localizations of nonheme ferric and ferrous iron in the rat brain: A light and electron microscopic study by the

- perfusion-perls and -turnbull methods. *Archiv Histol Cytol.* 2008; 71:205-222.
62. Uchida Y, Kan H, Sakurai K, et al. Iron leakage owing to blood-brain barrier disruption in small vessel disease CADASIL. *Neurology.* 2020;95:e1188.
 63. Righart R, Duering M, Gonik M, et al. Impact of regional cortical and subcortical changes on processing speed in cerebral small vessel disease. *NeuroImage Clin.* 2013;2:854-861.
 64. Duering M, Gonik M, Malik R, et al. Identification of a strategic brain network underlying processing speed deficits in vascular cognitive impairment. *NeuroImage.* 2013;66:177-183.
 65. Moore S, Meschkat M, Ruhwedel T, et al. A role of oligodendrocytes in information processing. *Nat Commun.* 2020;11:5497.
 66. Charlton RA, Morris RG, Nitkunan A, Markus HS. The cognitive profiles of CADASIL and sporadic small vessel disease. *Neurology.* 2006;66:1523-1526.
 67. Weiskopf N, Edwards LJ, Helms G, Mohammadi S, Kirilina EJNRP. Quantitative magnetic resonance imaging of brain anatomy and in vivo histology. *Nat Rev Phys.* 2021;3:570-588.
 68. Wardlaw JM, Benveniste H, Nedergaard M, et al. Perivascular spaces in the brain: Anatomy, physiology and pathology. *Nat Rev Neurol.* 2020;16:137-153.